

Research Article

***Plectranthus barbatus* Leaf Extract-Mediated Synthesis of ZnS and Mg-Doped ZnS NPs: Structural, Optical, Morphological, and Antibacterial Studies**

A. H. Al-Hammadi ¹, **Adnan Alnehaia** ¹, **Annas Al-Sharabi** ², **Abdel-Basit Al-Odayni** ³,
Naaser A. Y. Abdu ⁴, and **Waseem Sharaf Saeed** ³

¹Department of Physics, Faculty of Sciences, Sana'a University, Sana'a 12081, Yemen

²Department of Physics, Faculty of Applied Sciences, Thamar University, Dhamar 87246, Yemen

³Engineer Abdullah Bugshan Research Chair for Dental and Oral Rehabilitation, College of Dentistry, King Saud University, Riyadh 11545, Saudi Arabia

⁴Department of Chemistry, College of Science, King Saud University, P.O. Box 2455, Riyadh 11451, Saudi Arabia

Correspondence should be addressed to Adnan Alnehaia; ad.alnehaia@su.edu.ye and Abdel-Basit Al-Odayni; aalodayni@ksu.edu.sa

Received 3 May 2023; Revised 7 July 2023; Accepted 17 August 2023; Published 23 August 2023

Academic Editor: Dario Zappa

Copyright © 2023 A. H. Al-Hammadi et al. This is an open access article distributed under the Creative Commons Attribution License, which permits unrestricted use, distribution, and reproduction in any medium, provided the original work is properly cited.

In the current study, the researchers have explored the influence of doped Mg ions on the optical, morphological, and structural properties of zinc sulfide (ZnS) nanoparticles (NPs). The green technique was employed to prepare pure and 2% and 5% Mg-doped ZnS NPs using the *Plectranthus barbatus* leaf extract as a capping agent. XRD, SEM, FTIR, and UV-visible were used in the investigation process. The XRD results showed that all the synthesized materials have a cubic structure with space group F-43m. The D_{av} was nearly in the range of 2.02–2.20 nm. The SEM images illustrated that NPs were agglomerated. The UV-visible results showed that the optical bandgap increased as Mg^{2+} ions increased, which was in the range of 3.81–4.42 eV. The absorption shoulder of the prepared NPs is blue-shifted with increasing dopant concentration. The FTIR spectrum gives characteristic peaks for Zn-S bonds and asserts NPs' formation. The antibacterial check against *E. coli* and *S. aureus* bacterial strains revealed that pure and Mg-doped ZnS NPs have higher activity for both bacterial strains. The results have shown that the prepared materials can be used for antibacterial activities and optoelectronic applications.

1. Introduction

Among the family of semiconductor compounds, II–VI groups hold tremendous technological importance in many fields of science and technology. For instance, ZnS, CdS, ZnSe, CdTe, etc., are of great importance for solar cells and optoelectronics because they possess exceptional structural, electronic, and optical properties [1, 2]. The unique properties and applications of zinc sulfide (ZnS) nanoparticles (NPs) have recently made them one of the most promising research materials. It is a semiconductor with large band gap energy (3.68 eV at 298 K), wide exciton binding energy, and cubic unit cell with lattice constant $a = b = c = 5.406$ Å. Due

to their ability to demonstrate new properties when compared to bulk ZnS, NPs have garnered a lot of attention [3–8]. As a result of their excellent optoelectronic properties, low cost, nontoxicity, and natural abundance, ZnS NPs have been utilized for photocatalysts, solar cells, light diodes, and bio-applications [9–14], among others. Generally, chemical approaches for synthesizing nanomaterials are faster and cheaper, and they provide a higher yield than physical approaches. Therefore, such chemical methods are more suitable for industrial scales.

The literature review illustrates that ZnS NPs have been fabricated using different techniques involving sol-gel [15], coprecipitation [16, 17], solvothermal [18], green synthesis

[19], microwave [9], and hydrothermal techniques [20]. As it is well known, doping ZnS NPs with different metal atoms, especially alkaline earth metals, is an effective method of modifying the nanocrystals' optical properties and electrical properties [14, 21–23]. Furthermore, it is well known that NPs have a high surface-to-volume ratio, resulting in unstable properties when oxygen is chemisorbed at their surface in an ambient atmosphere leading to higher resistivity or uncontrolled luminescence emission. To overcome this obstacle, the surface bonds of the NPs can be adequately passivated with appropriate guest atoms, thereby promoting a stable state. Generally, choosing the suitable doping atom depends on the following criteria: (i) the ionic radius values of guest and host atoms should be similar and (ii) the thermal solubility limit should be as high as possible to maintain the high content of guest atoms [4, 24, 25]. Magnesium (Mg) ion is one possible doping atom, being a promising candidate to replace Zn sites in order to tune the optical properties of the host lattice.

In addition, Mg is a naturally abundant and low-toxic element. Moreover, due to its similar ionic radius to Zn, Mg ions are not expected to cause a significant lattice distortion of ZnS [26]. Indeed, doping ZnS NPs by various transition metals has been tried using different approaches [5, 15, 27, 28]. In the middle of these is the green method. It is an efficient approach to preparing ZnS NPs due to its simplicity and scalability. Several valuable reports regarding ZnS's structural, morphological, and optical properties have been published. For example, a work by Ashokkumar and Boopathyraja [11] has revealed that E_g gets increased with the increase in Mg dopant concentration. The results suggest that these materials can be used in optoelectronic applications [11]. Ayim-Otu et al. [29] have synthesized pure and (3%) Cu-doped ZnS NPs by coprecipitation, showing improved optical bandgap after doping and proving their possible use in photovoltaics [16]. According to the literature [11, 30, 31], doping of ZnS by Mg can be performed using different chemical processes; however, to the best of our knowledge, no research studies on using the *Plectranthus barbatus* (*P. barbatus*) leaf extract as a medium for the biosynthesis of Mg-doped ZnS NPs have been reported.

Herein, we focused on synthesizing ZnS pure and doped by Mg using the *P. barbatus* leaf extract as a capping agent. *P. barbatus* (also known as *Coleus forskohlii*) is a medicinal herb that belongs to Lamiaceae family and has proven its value as an antimicrobial, antioxidant, and antiseizure drug [32, 33]. Furthermore, it is used in herbal treatment of many diseases, including hypertension, congestive heart failure, eczema, colic, respiratory disorders, painful urination, insomnia, and convulsions [34]. The *P. barbatus* leaf extract has exhibited antibacterial, antioxidant, and immunomodulatory activities and were cytotoxic to gastric adenocarcinoma cells. The secondary metabolites of *P. barbatus* leaves have reported to include eugenol, α -pinene, and β -caryophyllene, which are toxic to larvae of *Anopheles subpictus*, *Stegomyia albopicta*, *Culex tritaeniorhynchus* [35], and *A. aegypti* fourth-instar larvae, but no insights into the mechanism of action have been reported [36]. A recent report has evaluated the phytochemical components in the

P. barbatus leaves from both aqueous and organic extracts. The main findings revealed the presence of flavonoids, cinnamic derivatives, steroids, and ellagic acid, with higher activity for the organic extract [37]. Plants of this species grow in many countries around the world, such as India, Ethiopia, Egypt, tropical East Africa, Yemen, and Brazil [32].

The effect of doping on the morphology, optical, and structural properties of ZnS was investigated, and furthermore, the antibacterial activities against Gram-positive and Gram-negative bacteria were assessed.

2. Materials and Methods

2.1. Materials. Zinc acetate dihydrate ($\text{Zn}(\text{CH}_3\text{OO})_2 \cdot 2\text{H}_2\text{O}$, 98.5%), sodium sulfide ($\text{Na}_2\text{S} \cdot x\text{H}_2\text{O}$; Himedia Laboratories 60%), magnesium nitrate hexahydrate ($\text{Mg}(\text{NO}_3)_2 \cdot 6\text{H}_2\text{O}$), and ethanol (EtOH, 99.8%) were purchased from BDH chemical Ltd. (Pool, England, UK). The bacteria strains (*Staphylococcus aureus* (*S. aureus*) and *Escherichia coli* (*E. coli*)) were kindly obtained as a gift from Al-Jarfi Medical Lab (Dhamar City, Yemen). Mueller–Hinton agar (MHA) was acquired from Sigma–Aldrich (Darmstadt, Germany) and used as recommended. Distilled water (DW) was used wherever.

2.2. Plant Collection. Fresh leaves of the target *P. barbatus* plant were collected from Dhamar valleys farms, Yemen. They were washed several times with tap water and DW. After that, the leaves were chopped into small pieces and crushed in a mortar with a pestle till they became dough [38].

2.3. Preparation of the Extract. 13 g of the dough-like crushed leaves were suspended in 200 mL DW. Then, the mixture was stirred for 90 min at 25°C, during which the color of the solution was changed from colorless to brown. After filtering, the resultant solution was immediately employed for production of the target pure and Mg-doped ZnS NPs [39].

2.4. Green Synthesis of ZnS NPs. To synthesize ZnS NPs, equal moles (3.5 moles) of $\text{Zn}(\text{CH}_3\text{OO})_2 \cdot 2\text{H}_2\text{O}$ and Na_2S were separately prepared in 25 mL each of the *P. barbatus* leaf extract (termed solutions A and B, respectively). Solution B was then added, in a dropwise manner, to solution A, and the mixture was stirred using a magnetic stirrer for 1 h at 25°C. After that, the product was filtered, washed with ethanol and DW, and dried at 25°C for 48 h. Finally, the obtained powder was further dried at 100°C for 1 h and then quashed into fine powder [39, 40]. The same procedure was repeated for doping ZnS with 2 and 5 mol% Mg. The overall scheme for the biosynthesis of ZnS and Mg-doped ZnS NPs and their bioactivity are summarized in Figure 1.

2.5. Antibacterial Test. The antibacterial effect of the prepared materials was executed for *S. aureus* (Gram-positive) and *E. coli* (Gram-negative) bacteria by the disc diffusion route [41, 42]. The concentrations of 70, 140, and 210 mg/mL

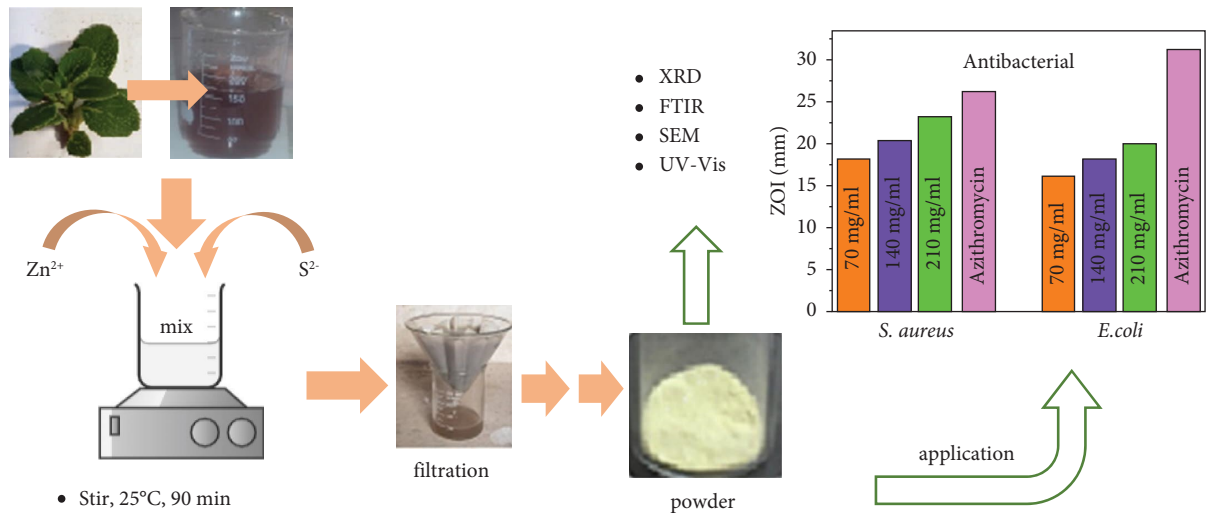


FIGURE 1: Schematic presentation for the biosynthesis route of ZnS and Mg-doped ZnS NPs using *Plectranthus barbatus* leaf extract, characterization methods, and bioactivity.

of the synthesized NPs were taken for the antibacterial check. The inhibition zones were measured after incubation at 36-37°C for 24 h.

2.6. Characterization. The X-ray diffraction (XRD) profiles for the pure and doped ZnS were recorded using an XD-2 X-ray diffractometer (Beijing, China) with $\text{CuK}\alpha$ radiation of $\lambda = 0.15418$ nm. Fourier transform infrared (FTIR) spectra were recorded via the Nicolet iS10 FTIR spectrometer from Thermo Scientific (Madison, WI, USA) on the range of 650–4000 cm^{-1} . The scanning electron micrograph (SEM) was imaged by JSM – 6360 LV (Tokyo, Japan). Electronic spectra were obtained using a Hitachi UV-vis U3900 spectrophotometer (Tokyo, Japan) coupled with Varian Cary-50 software and acquired in the range of 200–800 nm at room temperature. The NPs were suspended in DW and immediately analyzed using a 1 cm cuvette.

3. Results and Discussion

3.1. XRD Analysis. XRD analysis was employed to define the structural purity and crystallite size of the NPs. The XRD patterns for pure, 2% Mg, and 5% Mg-doped ZnS NPs are offered in Figure 2 and assured agreement PDF card no. 05-0566 [43]. Thus, three prominent peaks coinciding to (111), (220), and (311) planes of ZnS were observed, respectively, at 2θ of 28.75°, 48.01°, and 56.46°. The results revealed well-resolved patterns of ZnS NPs. The broadening in the diffraction peaks might be due to the size effect; therefore, the crystallite size is in the nanoregime. The average crystallite size (D) of the NPs is estimated by Debye Scherrer's relation $D = 0.9\lambda/\beta \cos \theta$ [4]. Bragg's formula was applied to estimated d -spacing $n\lambda = 2d \sin \theta$ [13], while the lattice parameter (a) was calculated using the equation $d = a/\sqrt{h^2 + k^2 + l^2}$ [43], where hkl is Miller's plans. The peak position (2θ), lattice parameter, d -spacing, and D_{ave} values for the highest intensity peak are collected in Table 1. From this table, it is found that the D value increases with the

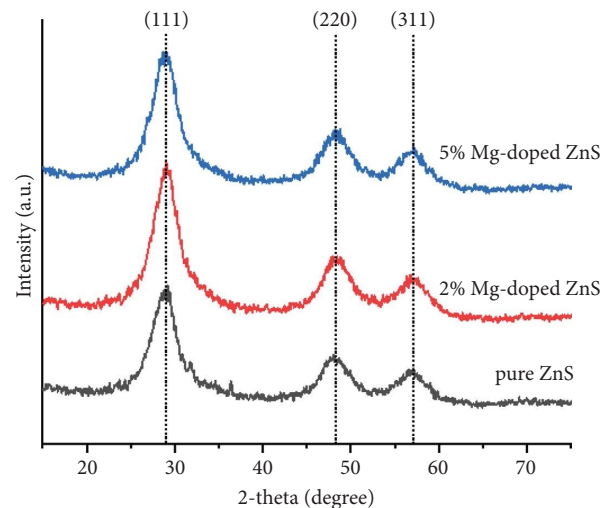


FIGURE 2: XRD spectra of pure and Mg-doped ZnS-NPs.

TABLE 1: The structure parameters of pure and Mg-doped ZnS NPs, which were calculated based on the most intense peak (111).

Doping ratio	2-Theta ₍₁₁₁₎ (degree)	Crystallite size (D ; nm)	d -spacing (Å)	a (Å)
0	28.747	2.021	3.103	5.375
0.02	28.947	2.166	3.082	5.338
0.05	28.822	2.204	3.095	5.361

increase in the Mg doper concentration, i.e., from 2.021 nm for the undoped ZnS to 2.204 nm for 0.05 Mg-doped ZnS. These results elucidate the role of the plant extract in facilitating the NPs' production.

Furthermore, it was observed that the position of the diffraction peak of (111) was slightly shifted to higher angles after doping, and it was proven that Mg is well superseded Zn in the ZnS matrix. The lattice (a) parameter and d -spacing values were slightly decreased due to the coalition of smaller ionic radii of Mg into the position of larger ionic

radii Zn [11]. The reduction in the parameter of lattice (a) and d -value lead peak position shifts into higher value. The slight increase in D_{ave} after Mg doping is due to the improvement of crystalline surface growth by the existence of Mg [11]. These results agree with the fact that has been reported by Ashokkumar and Boopathyrāja, who prepared pure and Mg-doped zinc sulfide using the coprecipitation method [11].

3.2. SEM Analysis. The SEM analysis was performed to study the surface morphology of the synthesized NPs. Figures 3(a) and 3(c) illustrate the SEM images of pure ZnS and 5% Mg-doped ZnS NPs. It can be seen that the NPs were irregular in shapes and sizes and agglomerated into higher clusters. Furthermore, it could be seen that the pure sample is less lumpy than the doped one, while the extent of particles' agglomeration was higher after doping. Due to the low magnification of the images, counting of the particles and particle sizes is difficult; however, the insert images (Figures 3(b) and 3(d)) could visualize traced particle sizes.

3.3. UV-Visible Spectroscopic Analysis. The UV-vis absorption spectra of Mg ions doped ZnS NPs are listed in the range 200–900 nm as shown in Figure 4(a). The pure and Mg-doped ZnS NPs revealed an absorbance shoulder at 321, 296, and 270 nm, respectively. In addition, it illustrates that the synthesized samples have excellent absorption at the short wavelength region. Also, it shows that the absorption shoulder of the prepared NPs shifts towards the shorter wavelengths as the concentration of the dopant increases. This can be explained by the strong $sp-d$ exchange interaction between the zinc sulfide band electrons and localized d spins related to the magnesium ions. The energy gap (E_g) for the synthesized NPs is computed using the relation $E_g = 1240/\lambda_c$ [44], where λ_c is the cut-off wavelength. The estimated E_g for the synthesized NPs was 3.86, 4.19, and 4.59 eV, respectively.

The Beer-Lambert formula was used to compute the absorption coefficient (α) [4] $\alpha = 2.303A/t$, where A and t represent the absorbance and the thickness, respectively. Figure 4(b) displays α for all the samples (pure and Mg-doped ZnS) as a function of wavelength (λ). It illustrates that α decreases as the λ increases. This made Mg-doped ZnS NPs an excellent nominee material for optoelectronic instruments as a window layer. Figure 4(c) displays the transmission spectra (T_s) of ZnS (pure), 2% Mg-doped ZnS, and 5% doped ZnS NPs. By incorporating Mg ions into the Zn-S lattice, distortions and imperfections are created, thereby suppressing transparency. This result was in coincidence with literature [11]. The extinction coefficient (k) as a function of λ for pure (ZnS) and Mg (0.02 and 0.05) doped ZnS NPs is shown in Figure 4. The k was computed via the equation $k = \alpha\lambda/4\pi$ [45].

Figure 4(c) shows that the extinction coefficient (k) at short wavelengths was increasing, and then as the wavelength increased, the k decreased up to 290 nm, and then a sudden increase was observed. Furthermore, as the wavelength increased, the k increased as well.

For a direct allowed transition, the E_g value was estimated using Tauc's equation (44). $(\alpha hv) = A(hv - E_g)^n$, where A is a constant, α is the absorption coefficient, hv is the incident photon energy, and n takes the values 1/2, 3/2, 2, and 3 depending on the material and the type of the optical transition whether it is direct or indirect by using $n = 1/2$. The estimated E_g is 3.81, 4.19, and 4.42 eV, respectively, as shown in Figure 5. These results are in a close agreement with previous studies reported by Mani et al. [19] and Ashokkumar and Boopathyrāja [11].

The E_g values obtained by applying both absorption edge and Tauc's equation methods were nearly equal. Accordingly, the E_g value of the NPs is larger than that of the bulk material. The increase in the E_g value of a semiconductor is due to the increase in the life-time of holes and electrons. Also, the observed E_g is blue-shifted, which can be attributed to the quantum confinement effects. Indeed, the reproducibility of the particle sizes and optical and other properties of bio-based NPs are challenging. Therefore, the primary concern to using the bio-synthetic route is to optimize the critical protocols. In certain case, the authors have reported a highly reproducible green method for the production of NPs as assessed by UV-visible spectroscopy [46]. However, this is not always the case, and extensive evaluation is needed.

3.4. FTIR Studies. FTIR spectra of the prepared pure ZnS, 2%, and 5% Mg-doped ZnS are shown in Figure 6. In principle, FTIR analysis helps in identifying the functional groups existing in the synthesized NPs as well as the various adsorbing chemical species. As can be seen, the spectra of pure ZnS and Mg-doped ZnS are nearly the same with a slight difference in some peak positions and intensities assigned to the variation in the crystals' nanostructures [47]. According to the literature [6, 47, 48], the peaks at 1127, 1109, and 617 cm^{-1} are due to Zn-S vibrations. After doping ZnS with Mg, a change in its microstructure is expected. The case could be followed through the change in the intensities of peaks at 1127 and 1109 cm^{-1} , thus supporting Mg inclusion into the main ZnS crystal [47]. The broad bands in the range of 3050–3670 cm^{-1} are due to HO stretching of the adsorbed water molecules on the surface of the nanocrystals [47]. It may also suggest absorption contributed from OH of alcohol and phenol of extract biomolecules. The strong bands at 1557, 1387, 1331, 1022, and 932 cm^{-1} could be assigned to the stretching bands of C=O, C=C, C-C, asymmetric C-O, and symmetric C-O which associated with the capping biomaterials, driving the production of ZnS and its doped Mg NPs [49].

3.5. Synthetic Mechanism. Based on the phytochemicals reported in the literature [37, 50], the reaction mechanism is depicted in Figure 7. Accordingly, flavonoids, cinnamic derivatives, steroids, terpenoids, saponins, and essential oils were major constituents of the *P. barbatus* leaf [50]. Notably, diterpenoids, including forskolin [51], plectranthone, and plectrinone [52], are one of the most bioactive compounds in the *P. barbatus* plant [33]. Hence, to simplify the illustration

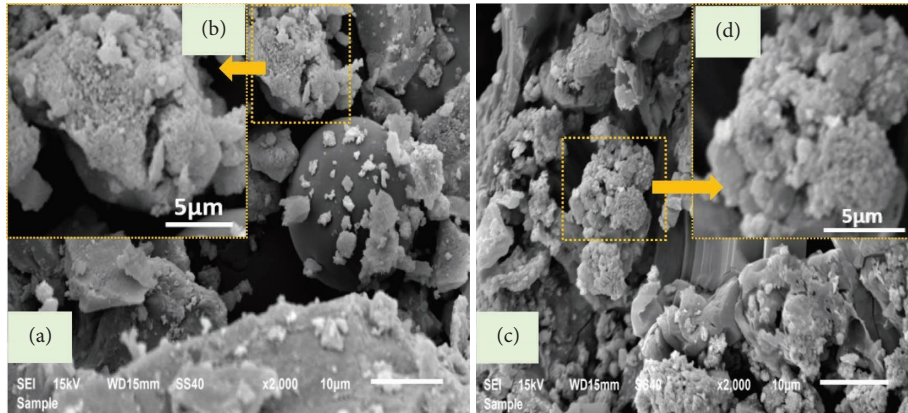


FIGURE 3: SEM micrographs of (a) pure ZnS and (c) 5% Mg-doped ZnS. (b) and (d) are magnification of the pointed area.

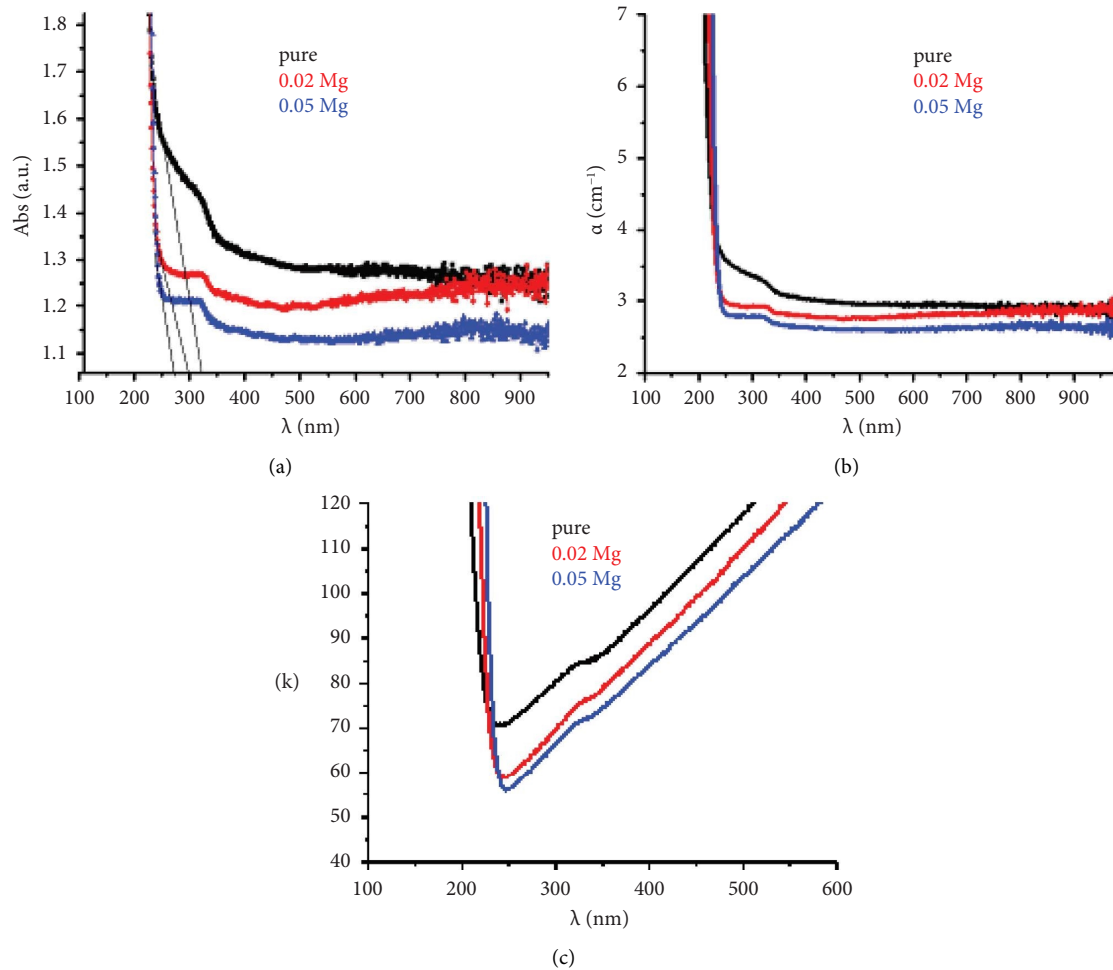


FIGURE 4: (a) Absorption spectra, (b) absorption coefficient (α), and (c) extinction coefficient k of ZnS (pure), 2%, and 5% Mg-doped ZnS NPs.

of the suggested mechanism, the diterpene called forskolin was used to represent the stabilizing agents used to prepare the target NPs (pure and Mg-doped ZnS NPs). As can be seen, forskolin combines several functional groups that

could contribute to capping and stabilizing ions for the next production of NPs. Hence, one forskolin molecule could coordinate as one, bi-, or multi-dentate with metal ions (Zn^{2+} and Mg^{2+}). On the other hand, essential oils and

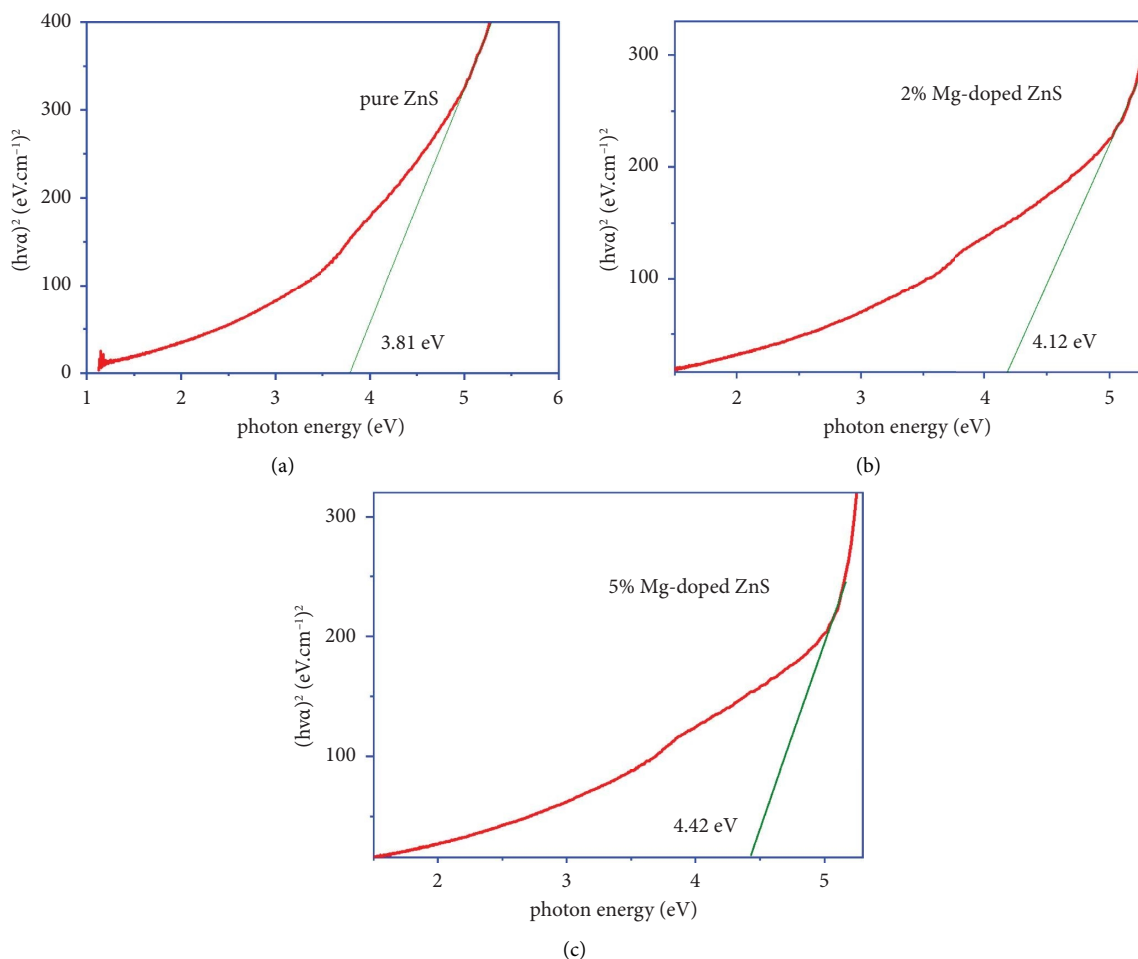


FIGURE 5: Optical bandgap energy for (a) pure ZnS, (b) 0.02 Mg-doped ZnS, and (c) 0.05-Mg doped ZnS NPs.

amino acids can stabilize the sulfide ions. Thus, by further hydrolysis of the coordinated ions, the end NPs can be obtained [53].

3.6. Antibacterial Studies. The antibacterial effect of the as-prepared pure and (0.02, 0.05) Mg-doped ZnS NPs was investigated against *S. aureus* and *E. coli* strains to check their utility as potential materials for biological applications. Figures 8(a) and 8(b) show the zone of inhibition (ZOI), and Table 2 displays the measured ZOI for all the prepared compounds. The results indicated higher antibacterial potency of pure ZnS NPs than the Mg-doped one, with lesser activity against Gram-negative than Gram-positive bacteria. The difference can be explicated by the chemical composition and various structures of each cell surfaces, as the cell wall of Gram-positive and Gram-negative bacteria is different [54, 55]. The higher activity is due to the greater ability of prepared NPs to generate reactive oxygen species, which leads to oxidative stress and destruction of bacterial cells [11, 56]. According to previous studies, several mechanisms could be proposed for the antibacterial resistance of NPs. Due to smaller sizes of NPs, they can easily adhere with the cell wall of the bacterium and can cause destruction, which

will lead to the death of the cell. The electrostatic interaction of the nanomaterials with the cell wall and photocatalytic light activation are also a common possible reason behind the antibacterial activity of nanomaterials [57, 58].

The antibacterial activity of the *P. barbatus* extract has been reported to be solvent-dependent, with the aqueous extract effect being lower than the organic one [37]. In the present study, the experiment was performed to evaluate the antibacterial activity of the synthesized inorganic NPs; however, the plant extract was not targeted and thus was not compared. It is worth mentioning that even though a trace of the plant phytochemicals can be detected, their effect would not be counted due to the traced concentration. On the other hand, the antibacterial activity of chemically synthesized ZnS NPs is low, as reported elsewhere [59], supporting the advantage of the biosynthesis method in producing NPs with a better performance against microbes.

According to Ashokkumar and Boopathyraja [11], the antibacterial activity of ZnS NPs prepared via a coprecipitation method was dopant-ratio dependent; however, the case was not straightforward, and instead, a peak of efficacy was found at 0.2Mg-doped ZnS among the tested (0.0–0.4)Mg-doped ZnS NPs. A similar trend was seen for ZnS-filled polyvinylpyrrolidone/Chitosan [60] against *S. aureus* and

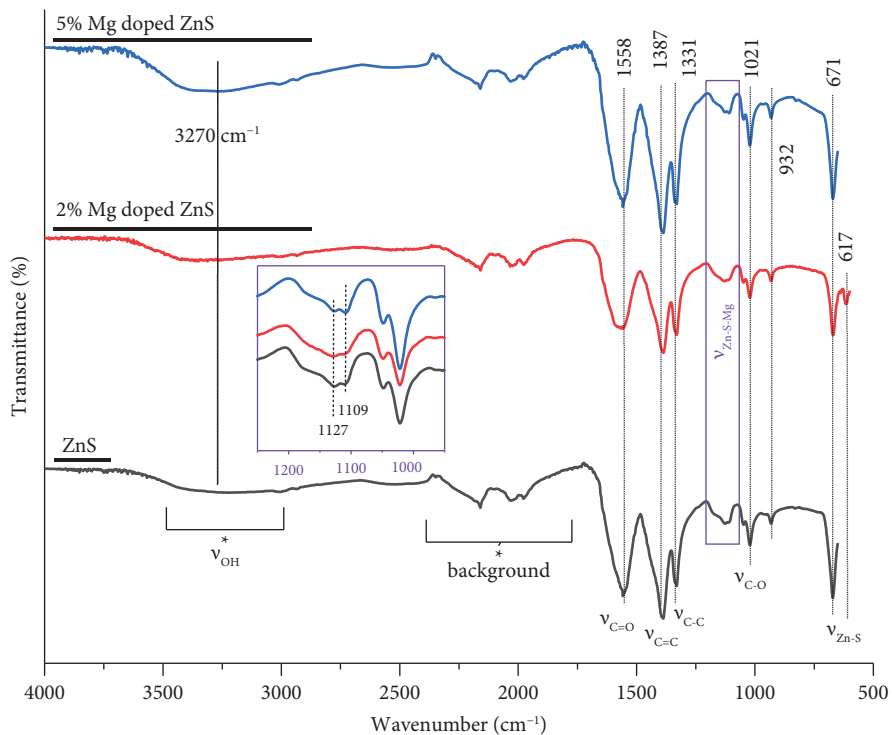


FIGURE 6: FTIR spectra of ZnS and Mg-doped ZnS. The insert is an overlay illustrating the intensity difference of the peaks at 1109 and 1127 cm^{-1} associated with the doping effect.

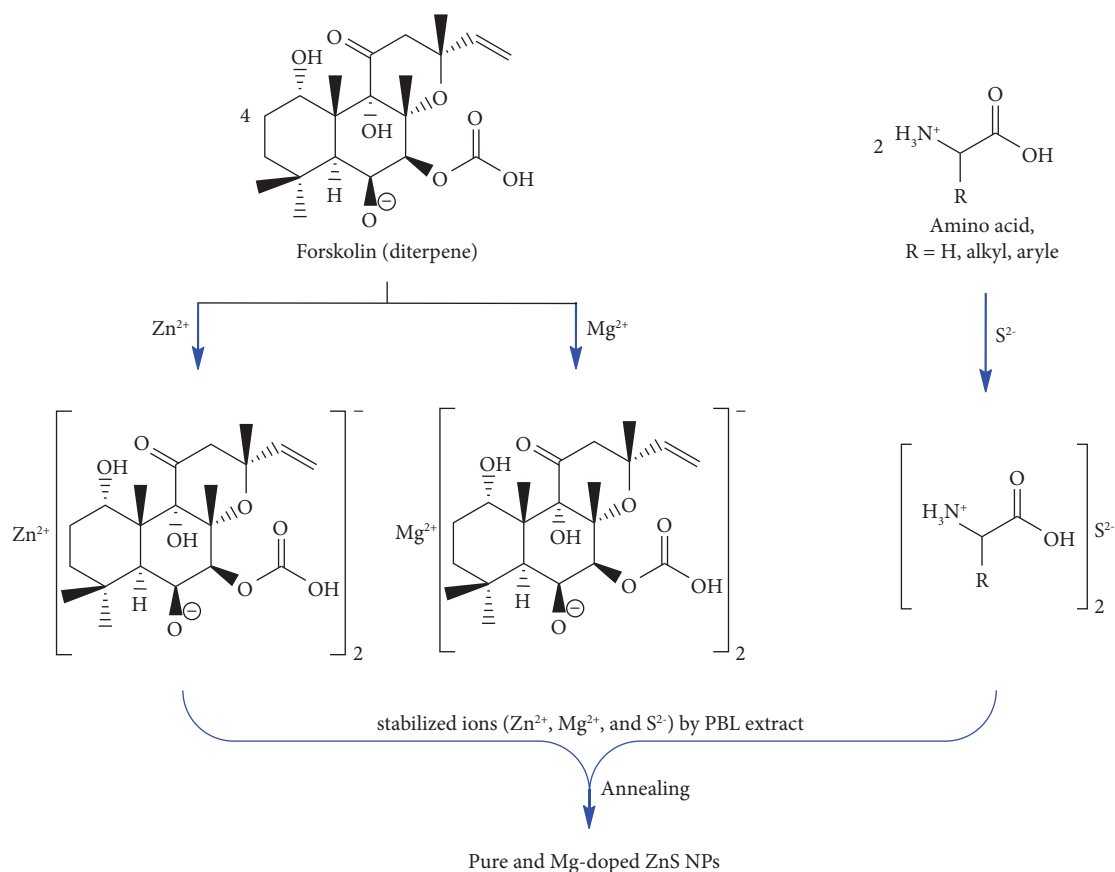


FIGURE 7: Schematic presentation of the proposed mechanism for the phytosynthesis of Mg-doped ZnS using *Plectranthus barbatus* leaf (PBL) extract.

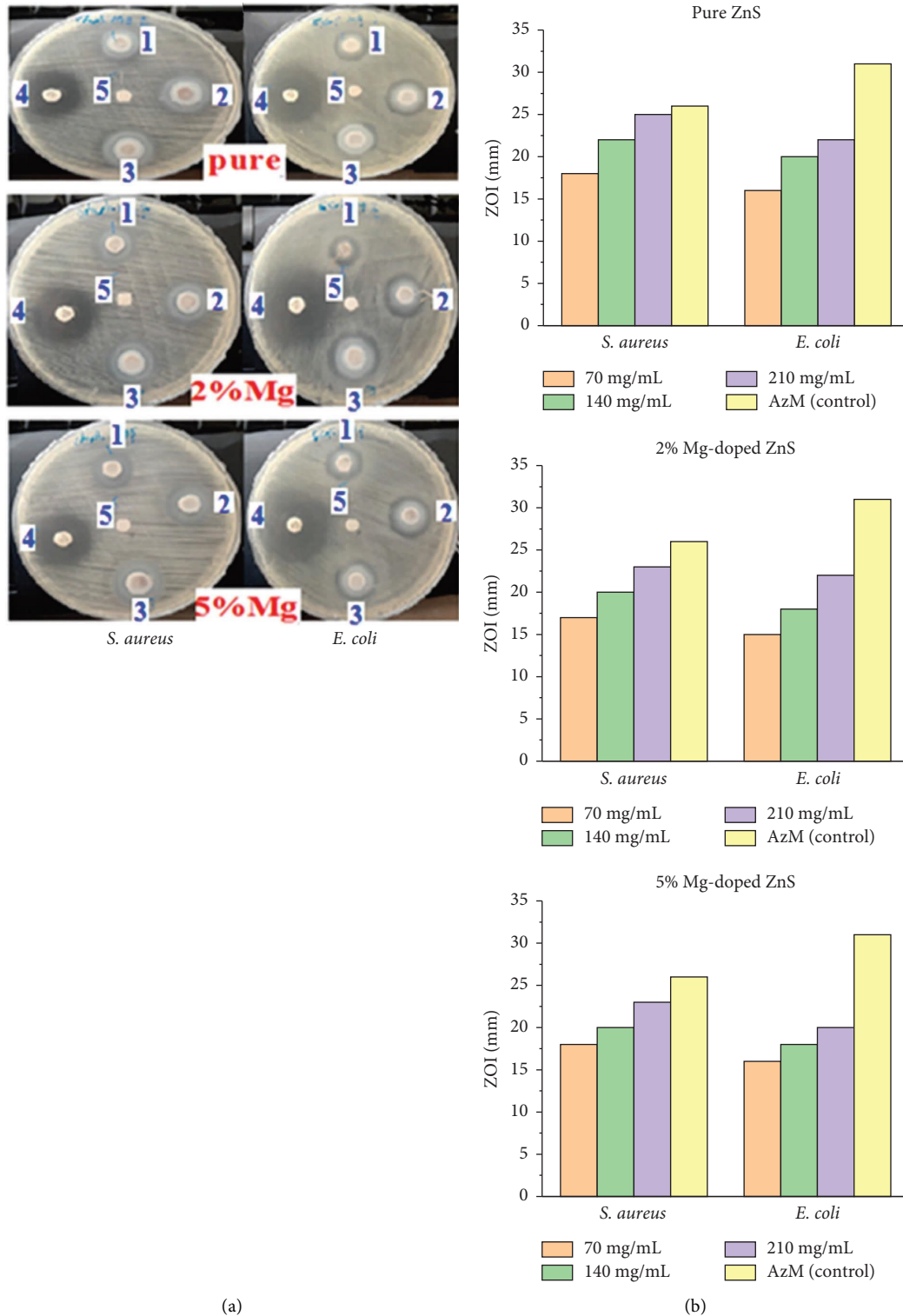


FIGURE 8: (a) Antibacterial activity of pure, 2%, and 5% Mg-doped ZnS NPs against Gram-negative bacteria (*E. coli*) and Gram-positive bacteria (*S. aureus*). (1) 70 mg/mL per disc, (2) 140 mg/mL per disc, (3) 210 mg/mL per disc, (4) azithromycin antibiotics (positive control), and (5) distilled water (negative control). (b) Histogram illustration for the corresponding zone of inhibition data.

E. coli, demonstrating a concentration-dependent activity that is higher against *S. aureus*. The ZOI against *S. aureus* and *E. coli* was reported as the greatest among a list of bacterium strains investigated by Segura et al. [61]; however, the study

indicated closer susceptibility of both bacteria for ZnS at higher concentrations. It is also reported that other kinds of ZnS nanostructures synthesized by chemical and green methods have shown efficient antibacterial activity against

TABLE 2: Antibacterial activity of fabricated pure ZnS, 2%, and 5% Mg-doped ZnS NPs.

Sample	Bacteria	Zone of inhibition (ZOI; mm) at various concentrations			
		70 mg/mL	140 mg/mL	210 mg/mL	Azithromycin (control)
Pure ZnS	<i>S. aureus</i>	18	22	25	26
	<i>E. coli</i>	16	20	22	31
2% Mg-doped ZnS	<i>S. aureus</i>	17	20	23	26
	<i>E. coli</i>	15	18	22	31
5% Mg-doped ZnS	<i>S. aureus</i>	18	20	23	26
	<i>E. coli</i>	16	18	20	31

both strains, exhibiting similar ZOI at similar concentrations [59, 62, 63]. Despite the synthesis method, the antibacterial activity of doped ZnS NPs varies depending on the dopant type and concentration. Hence, Ag-doping has enhanced the ZnS activity [64], Mg-doped ZnS has an optimal value [11], and Sn-doping showed the same or slightly lesser activity than pure ZnS [63]. The latter one supports our findings that the activity of pure ZnS is marginally higher activity than that of Mg-doped ones. Such differences are brought about by the various sizes and shapes present in each doped ZnS product, which in turn rely on the synthesis method.

4. Conclusion

In this paper, pure and (2% and 5%) Mg-doped ZnS NPs were successfully prepared via an economical, easy, and environment-friendly route using the *P. barbatus* leaf extract. The XRD pattern proved the cubic phase with crystallite sizes in the range of 2.02–2.204 nm. The SEM revealed that the obtained NPs are agglomerated. The UV-visible results have shown that the optical band gap was increased as Mg²⁺ ions increased, which were in the range 3.81–4.42 eV. The FTIR study denotes the existence of OH, C-C, and C=O functional groups which are the surface-active molecules that stabilize the ZnS NPs. The antibacterial test demonstrated that the biosynthesized pure ZnS and Mg-doped ZnS NPs had remarkable inhibition of growth of both Gram-negative and Gram-positive bacteria.

Data Availability

The data used to support the findings of this study are included within the article.

Conflicts of Interest

The authors declare that they have no conflicts of interest.

Authors' Contributions

All of the authors mentioned contributed significantly to the development and writing of the paper.

Acknowledgments

The authors extend their appreciation to the Deputyship for Research & Innovation, Ministry of Education in Saudi Arabia, for funding this research (IFKSURC-1-1910).

References

- [1] R. Cingolani, M. Lomascolo, N. Lovergine, M. Dabiccio, M. Ferrara, and I. Suemune, "Excitonic properties of ZnSe/ZnSeS superlattices," *Applied Physics Letters*, vol. 64, no. 18, pp. 2439–2441, 1994.
- [2] K. Deka and M. P. C. Kalita, "Structural, optical and ion sensing properties of 2-mercaptoethanol capped Mn-doped ZnS nanocrystals," *Superlattices and Microstructures*, vol. 111, pp. 373–384, 2017.
- [3] R. Sahraei, F. Mohammadi, E. Soheyli, and M. Roushani, "Synthesis and photoluminescence properties of Ru doped ZnS quantum dots," *Journal of Luminescence*, vol. 187, pp. 421–427, 2017.
- [4] A. Al-Osta, A. Alnehia, A. A. Qaid, H. T. Al-Ahsab, and A. Al-Sharabi, "Structural, morphological and optical properties of Cr doped ZnS nanoparticles prepared without any capping agent," *Optik*, vol. 214, Article ID 164831, 2020.
- [5] S. Kannan, N. P. Subramaniam, and M. Sathishkumar, "A novel green synthesis approach for improved photocatalytic activity and antibacterial properties of zinc sulfide nanoparticles using plant extract of *Acalypha indica* and *Tridax procumbens*," *Journal of Materials Science: Materials in Electronics*, vol. 31, no. 12, pp. 9846–9859, 2020.
- [6] A. Dhupar, S. Kumar, H. S. Tuli, A. K. Sharma, V. Sharma, and J. K. Sharma, "In-doped ZnS nanoparticles: structural, morphological, optical and antibacterial properties," *Applied Physics A*, vol. 127, no. 4, pp. 263–274, 2021.
- [7] P. Sakthivel and S. Muthukumar, "Structural, photoluminescence and magnetic properties of Mn, Cr dual-doped ZnS quantum dots: influence of Cr concentration," *Journal of Physics and Chemistry of Solids*, vol. 120, pp. 183–189, 2018.
- [8] P. Sakthivel and S. Muthukumar, "Influence of Co²⁺ on electrical and optical behavior of Mn²⁺-doped ZnS quantum dots," *Optics and Laser Technology*, vol. 103, pp. 109–117, 2018.
- [9] D. Ayodhya and G. Veerabhadram, "Microwave-assisted synthesis, characterization and photoluminescence interaction studies of undoped, Zr⁴⁺, Rh³⁺ and Pd²⁺ doped ZnS quantum dots," *Materials Discovery*, vol. 12, pp. 1–8, 2018.
- [10] S. Horoz, "Cr kknkföi," *Iğdır Üniversitesi Fen Bilimleri Enstitüsü Dergisi*, vol. 8, no. 2, pp. 89–97, 2018.
- [11] M. Ashokkumar and A. Boopathyraja, "Structural and optical properties of Mg doped ZnS quantum dots and biological applications," *Superlattices and Microstructures*, vol. 113, pp. 236–243, 2018.
- [12] Y. Al-Douri, K. D. Verma, and D. Prakash, "Optical investigations of blue shift in ZnS quantum dots," *Superlattices and Microstructures*, vol. 88, pp. 662–667, 2015.
- [13] A. Al-Sharabi, A. Alnehia, A. Al-Osta, and N. A. A. Yahya, "Effect of copper doping on structural and optical properties

- of zinc sulfide (zns) nanoparticles,” *Al-Baydha University Journal for Researches*, vol. 1, pp. 224–234, 2019.
- [14] S. Horoz, Q. Dai, F. S. Maloney et al., “Absorption induced by mn doping of zns for improved sensitized quantum-dot solar cells,” *Physical Review Applied*, vol. 3, no. 2, Article ID 024011, 2015.
- [15] M. Sathishkumar, M. Saroja, and M. Venkatachalam, “Influence of (Cu, Al) doping concentration on the structural, optical and antimicrobial activity of ZnS thin films prepared by Sol-Gel dip coating techniques,” *Optik*, vol. 182, pp. 774–785, 2019.
- [16] B. A. Otu, M. Kuncan, O. Şahin, and S. Horoz, “Synthesis and photovoltaic application of ZnS:Cu (3%) nanoparticles,” *Australian Ceramic Society*, vol. 56, 2019.
- [17] J. K. Salem, T. M. Hammad, S. Kuhn et al., “Structural and optical properties of Co-doped ZnS nanoparticles synthesized by a capping agent,” *Journal of Materials Science: Materials in Electronics*, vol. 25, no. 5, pp. 2177–2182, 2014.
- [18] S. M. El-Hamidy, “The optical behavior of multi-emission quantum dots based on Tb-doped ZnS developed via solvothermal route for bioimaging applications,” *Optik*, vol. 207, Article ID 163868, 2020.
- [19] S. K. Mani, S. Manickam, V. Muthusamy, and R. Thangaraj, “Antimicrobial activity and photocatalytic degradation properties of zinc sulfide nanoparticles synthesized by using plant extracts,” *Journal Nanostruct*, vol. 8, pp. 107–118, 2018.
- [20] C. Li, H. Chen, M. Ivanov et al., “Large-scale hydrothermal synthesis and optical properties of Cr²⁺:ZnS nanocrystals Ceramics,” *Ceramics International*, vol. 44, no. 11, pp. 13169–13175, 2018.
- [21] J. K. Salem, T. M. Hammad, S. Kuhn et al., “Luminescence properties of Mn and Ni doped ZnS nanoparticles synthesized by capping agent,” *Journal of Materials Science: Materials in Electronics*, vol. 25, no. 12, pp. 5188–5194, 2014.
- [22] B. Sreenivasulu, S. Venkatramana Reddy, and P. Venkateswara Reddy, “Structural, optical and magnetic properties of (Cu, Ni) co-doped ZnS nanoparticles,” *Journal of Materials Science: Materials in Electronics*, vol. 29, no. 1, pp. 251–259, 2017.
- [23] K. Bera, S. Saha, and P. Chandra Jana, “Investigation of Structural and Electrical properties of ZnS and Mn doped ZnS nanoparticle,” *Materials Today: Proceedings*, vol. 5, no. 2, pp. 6321–6328, 2018.
- [24] D. Amaranatha Reddy, A. Divya, G. Murali, R. P. Vijayalakshmi, and B. K. Reddy, “Synthesis and optical properties of Cr doped ZnS nanoparticles capped by 2-mercaptoethanol,” *Physica B: Condensed Matter*, vol. 406, no. 10, pp. 1944–1949, 2011.
- [25] M. S. Nadeem, T. Munawar, F. Mukhtar et al., “Hydrothermally derived co, Ni co-doped ZnO nanorods; structural, optical, and morphological study,” *Optical Materials*, vol. 111, Article ID 110606, 2021.
- [26] R. D. Shannon, “Revised effective ionic radii and systematic studies of interatomic distances in halides and chalcogenides,” *Acta Crystallographica Section A*, vol. 32, no. 5, pp. 751–767, 1976.
- [27] S. J. Basha, V. Khidhirbrahmendra, M. Avinash, N. B. Reddy, G. V. Zyryanov, and R. V. S. S. N. Ravikumar, “Structural, magnetic and thermal properties of Mn²⁺ doped ZnS nanocrystals for device applications,” in *Proceedings of the AIP Conference Proceeding 2063*, Long Island, NY, USA, January 2019.
- [28] J. Sharma, A. Gupta, and O. P. Pandey, “Effect of Zr doping and aging on optical and photocatalytic properties of ZnS nanopowder,” *Ceramics International*, vol. 45, no. 11, pp. 13671–13678, 2019.
- [29] B. Ayim-Otu, M. Kuncan, O. Şahin, and S. Horoz, “Synthesis and photovoltaic application of ZnS: Cu (3%) nanoparticles,” *Journal of the Australian Ceramic Society*, vol. 56, no. 2, pp. 639–643, 2020.
- [30] I. Ali, Z. A. Alothman, and A. Alwarthan, “Uptake of propranolol on ionic liquid iron nanocomposite adsorbent: kinetic, thermodynamics and mechanism of adsorption,” *Journal of Molecular Liquids*, vol. 236, pp. 205–213, 2017.
- [31] J. A. Abd, “Structural, morphological and optical properties of mg: zns nanoparticle for future contribution in different biological uses,” *Journal of Global Pharma Technology*, vol. 9, 2009.
- [32] W. A. de Almeida, I. C. V. Nova, J. D. Nascimento et al., “Effects of *Plectranthus barbatus* leaf extract on survival, digestive proteases, midgut morphophysiology and gut microbiota homeostasis of *Aedes aegypti* larvae,” *South African Journal of Botany*, vol. 141, pp. 116–125, 2021.
- [33] L. C. Borges Fernandes, C. Campos Câmara, and B. Soto-Blanco, “Anticonvulsant activity of extracts of *Plectranthus barbatus* leaves in mice,” *Evidence-based Complementary and Alternative Medicine*, vol. 2012, Article ID 860153, 4 pages, 2012.
- [34] K. Kulbat-Warycha, J. Oracz, and D. Żyżelewicz, “Bioactive properties of extracts from *Plectranthus barbatus* (Coleus forskohlii) roots received using various extraction methods,” *Molecules*, vol. 27, no. 24, p. 8986, 2022.
- [35] M. Govindarajan, M. Rajeswary, S. Hoti, A. Bhattacharyya, and G. Benelli, “Eugenol, α -pinene and β -caryophyllene from *Plectranthus barbatus* essential oil as eco-friendly larvicides against malaria, dengue and Japanese encephalitis mosquito vectors,” *Parasitology Research*, vol. 115, no. 2, pp. 807–815, 2016.
- [36] J. K. Musau, J. M. Mbaria, J. M. Nguta, M. Mathiu, and S. G. Kiama, *Phytochemical Composition and Larvicidal Properties of Plants Used for Mosquito Control in Kwale County*, University of Nairobi, Nairobi, Kenya, 2016.
- [37] M. Cordeiro, T. Nunes, F. Bezerra et al., “Phytochemical characterization and biological activities of *Plectranthus barbatus* Andrews,” *Brazilian Journal of Biology*, vol. 82, Article ID e236297, 2021.
- [38] M. M. Khan, M. H. Harunsani, A. L. Tan, M. Hojamberdiev, Y. A. Poi, and N. Ahmad, “Antibacterial studies of ZnO and Cu-doped ZnO nanoparticles synthesized using aqueous leaf extract of *Stachytarpheta jamaicensis*,” *BioNanoScience*, vol. 10, no. 4, pp. 1037–1048, 2020.
- [39] A. Rahman, A. L. Tan, M. H. Harunsani, N. Ahmad, M. Hojamberdiev, and M. M. Khan, “Visible light induced antibacterial and antioxidant studies of ZnO and Cu-doped ZnO fabricated using aqueous leaf extract of *Ziziphys mauritiana* Lam,” *Journal of Environmental Chemical Engineering*, vol. 9, no. 4, Article ID 105481, 2021.
- [40] A. Rahman, M. H. Harunsani, A. L. Tan, N. Ahmad, M. Hojamberdiev, and M. M. Khan, “Effect of mg doping znO fabricated using aqueous leaf extract of *Ziziphys mauritiana* lam. for antioxidant and antibacterial studies,” *Bioprocess and Biosystems Engineering*, vol. 44, 2021.
- [41] W. Ahmad and D. Kalra, “Green synthesis, characterization and anti microbial activities of ZnO nanoparticles using *Euphorbia hirta* leaf extract,” *Journal of King Saud University Science*, vol. 32, no. 4, pp. 2358–2364, 2020.

- [42] A. Alnehia, A. Al-Sharabi, A. H. Al-Hammadi, A.-B. Al-Odayni, S. A. Alramadhan, and R. M. Alodeni, "Phyto-mediated synthesis of silver-doped zinc oxide nanoparticles from plectranthus barbatus leaf extract: optical, morphological, and antibacterial properties," *Biomass Conversion and Biorefinery*, vol. 10, 2023.
- [43] A. B. Alwany, G. M. Youssef, E. E. Saleh, O. M. Samir, M. A. Algradee, and A. Alnehia, "Structural, optical and radiation shielding properties of ZnS nanoparticles QDs," *Optik*, vol. 260, Article ID 169124, 2022.
- [44] S. J. Basha, V. Khidhirbrahmendra, J. Madhavi, U. U. Thampy, C. V. Reddy, and R. V. S. S. N. Ravikumar, "Structural, optical, magnetic and thermal investigations on Cr³⁺ ions doped ZnS nanocrystals by co-precipitation method," *Journal of Science: Advanced Materials and Devices*, vol. 4, no. 2, pp. 260–266, 2019.
- [45] C. Belkhaoui, N. Mzabi, and H. Smaoui, "Investigations on structural, optical and dielectric properties of Mn doped ZnO nanoparticles synthesized by co-precipitation method," *Materials Research Bulletin*, vol. 111, pp. 70–79, 2019.
- [46] D. Lomeli-Marroquín, D. Medina Cruz, A. Nieto-Argüello et al., "Starch-mediated synthesis of mono- and bimetallic silver/gold nanoparticles as antimicrobial and anticancer agents," *International Journal of Nanomedicine*, vol. 14, pp. 2171–2190, 2019.
- [47] S. Ummartyotin, N. Bunnak, J. Juntaro, M. Sain, and H. Manuspiya, "Synthesis and luminescence properties of ZnS and metal (Mn, Cu)-doped-ZnS ceramic powder," *Solid State Sciences*, vol. 14, no. 3, pp. 299–304, 2012.
- [48] B. S. Rema Devi, R. Raveendran, and A. Vaidyan, "Synthesis and characterization of Mn²⁺-doped ZnS nanoparticles," *Pramana*, vol. 68, no. 4, pp. 679–687, 2007.
- [49] P. V. Raleaooa, A. Roodt, G. G. Mhlongo, D. E. Motaung, R. E. Kroon, and O. M. Ntwaeaborwa, "Luminescent, magnetic and optical properties of ZnO-ZnS nanocomposites," *Physica B: Condensed Matter*, vol. 507, pp. 13–20, 2017.
- [50] J. O. Ezeonwumelu, G. N. Kawooya, A. G. Okoruwa et al., "Phytochemical screening, toxicity, analgesic and anti-pyretic studies of aqueous leaf extract of *Plectranthus barbatus* in rats," *Pharmacology and Pharmacy*, vol. 10, no. 4, pp. 205–221, 2019.
- [51] L. Valdes, S. Mislankar, and A. Paul, "Coleus barbatus (*C. forskohlii*) (Lamiaceae) and the potential new drug forskolin (Coleonol)," *Economic Botany*, vol. 41, no. 4, pp. 474–483, 1987.
- [52] M. Abdel-Mogib, H. Albar, and S. Batterjee, "Chemistry of the genus *Plectranthus*," *Molecules*, vol. 7, no. 2, pp. 271–301, 2002.
- [53] A. Alnehia, A. Al-Sharabi, A. Al-Hammadi, A.-B. Al-Odayni, W. S. Saeed, and A. Alrahlah, "Structural, optical, and bio-activity properties of silver-doped zinc sulfide nanoparticles synthesized using *Plectranthus barbatus* leaf extract," *Journal of Chemistry*, vol. 2023, Article ID 1399703, 10 pages, 2023.
- [54] A. Alnehia, A. H. Al-Hammadi, A. Al-Sharabi, and H. Alnahari, "Optical, structural and morphological properties of ZnO and Fe³⁺ doped ZnO-NPs prepared by *Foeniculum vulgare* extract as capping agent for optoelectronic applications," *Inorganic Chemistry Communications*, vol. 143, Article ID 109699, 2022.
- [55] A. Al-Sharabi, A. Alnehia, A. H. Al-Hammadi, K. A. Alhumaidha, and A. Al-Osta, "The effect of *Nigella sativa* seed extract concentration on crystal structure, band gap and antibacterial activity of ZnS-NPs prepared by green route," *Journal of Materials Science: Materials in Electronics*, vol. 33, no. 26, pp. 20812–20822, 2022.
- [56] A. Al-Sharabi, K. S. S. Sada'a, A. Al-Osta, and R. Abd-Shukor, "Structure, optical properties and antimicrobial activities of MgO-Bi_{2-x}Cr_xO nanocomposites prepared via solvent-deicent method," *Scientific Reports*, vol. 12, no. 1, Article ID 10647, 2022.
- [57] M. Y. Jehad and N. D. Enas, "Invitro antibacterial activity and minimum inhibitory concentration of zinc oxide and nanoparticle zinco xide against pathogenic strains," *Journal of Health Science*, vol. 12, pp. 38–42, 2012.
- [58] V. B. Schwartz, F. Thétiot, S. Ritz et al., "Antibacterial surface coatings from zinc oxide nanoparticles embedded in poly (Nisopropyla- crylamide) hydrogel surface layers," *Advances in Functional Materials*, vol. 22, no. 11, pp. 2376–2386, 2012.
- [59] S. Vijayan, C. S. Dash, G. Umadevi, M. Sundararajan, and R. Mariappan, "Investigation of structural, optical and antibacterial activity of ZnS nanoparticles," *Journal of Cluster Science*, vol. 32, no. 6, pp. 1601–1608, 2021.
- [60] M. A. Aboelwafa, A. M. Abdelghany, and M. S. Meikhal, "Preparation, characterization, and antibacterial activity of ZnS-NP's filled polyvinylpyrrolidone/chitosan thin films," *Biointerface Research in Applied Chemistry*, vol. 11, pp. 14336–14343, 2021.
- [61] A. Segura, A. Rodriguez, P. Hernández et al., "Sulfidogenic bioreactor-mediated formation of ZnS nanoparticles with antimicrobial and photocatalytic activity," *Nanomaterials*, vol. 13, no. 5, p. 935, 2023.
- [62] S. K. Mani, M. Saroja, M. Venkatachalam, and T. Rajamanickam, "Antimicrobial activity and photocatalytic degradation properties of zinc sulfide nanoparticles synthesized by using plant extracts," *Journal of Nanostructures*, vol. 8, pp. 107–118, 2018.
- [63] R. Kumar, P. Sakthivel, and P. Mani, "Structural, optical, electrochemical, and antibacterial features of ZnS nanoparticles: incorporation of Sn," *Applied Physics A*, vol. 125, no. 8, p. 543, 2019.
- [64] S. Pourmoslemi, F. Seif, and R. Mahjub, "Enhanced antibacterial activity of Ag-doped ZnS nanoparticles synthesised by a microwave-assisted polyol method," *Materials Research Innovations*, vol. 25, no. 7, pp. 399–403, 2021.